Biosensors

DOI: 10.1002/ange.201303420

Semiconducting Polymer Nanoprobe for In Vivo Imaging of Reactive Oxygen and Nitrogen Species**

*Kanyi Pu, Adam J. Shuhendler, and Jianghong Rao**

The elevated generation of reactive oxygen and nitrogen species (RONS) is a hallmark of many pathological processes ranging from acute and chronic bacterial infections to chronic diseases such as cancer, cardiovascular disease, and arthritis.[1] Therefore, the ability to detect the generation of RONS as pathological chemical messengers is critical to both understanding the etiology of these diseases and optimizing therapeutic interventions. Many fluorescent RONS sensing probes[2] have been developed including small-molecule fluorophores,[3] genetically encoded proteins,[4] single-walled carbon nanotubes (SWCNs),[5] quantum dots (QDs),[6] and dye-conjugated inorganic nanoparticles;[7] however, probes applicable for in vivo imaging are still very limited.[2]

In addition to near-infrared (NIR) fluorescence, one of the most important prerequisites for in vivo RONS imaging is the resistance of the reporter moiety of the probe to degradation by RONS. Failing to meet this requirement will likely result in a greatly reduced signal-to-noise ratio because persistent microenvironmental RONS in vivo will bleach the activated probe and lead to false negative signals. QDs and many small-molecule dyes are not stable in the presence of highly oxidative RONS such as hypochlorite (ClO^-),[6,8] and thus are not ideal to serve as the signal output units in this application of imaging probes.

Semiconducting polymer nanoparticles (SPNs) represent a new class of photostable fluorescent nanomaterials with excellent brightness that can be orders of magnitude higher than that of small-molecule fluorophores, and tens of times better than that of QDs.[9] As these nanoparticles are primarily composed of π-conjugated polymers, their use as fluorescent probes eliminates the possibility of heavy metal ion-induced toxicity to living organisms, potentially giving rise to good biocompatibility.[10] Despite these advantages, examples of SPNs in in vivo molecular imaging are still very few.[11] Recently, we have developed a bioluminescence resonance energy transfer (BRET) and fluorescence resonance energy transfer (FRET) relay nanoprobe for lymph node mapping and tumor imaging by taking advantage of the efficient light-harvesting properties of SPNs.[12] In addition, SPNs are shown to maintain its fluorescence in the presence of H_2O_2 and ClO^-.[9d] All these optical and physiological advantages of SPNs make them a promising nanoplatform for in vivo RONS imaging.

We herein report a dual-color SPN-based NIR nanoprobe for the detection of RONS (in short, NanoDRONE) in inflammatory microenvironments in living mice. NanoDRONE is designed to comprise a RONS-inert SPN core (energy donor) covered by RONS-sensitive fluorophore molecules (energy acceptors), enabling FRET from the SPN core to the fluorophore in the absence of RONS (Figure 1a). The presence of RONS can decompose the energy-accepting fluorophore and subsequently abolish the FRET within NanoDRONE, ultimately leading to enhanced emission

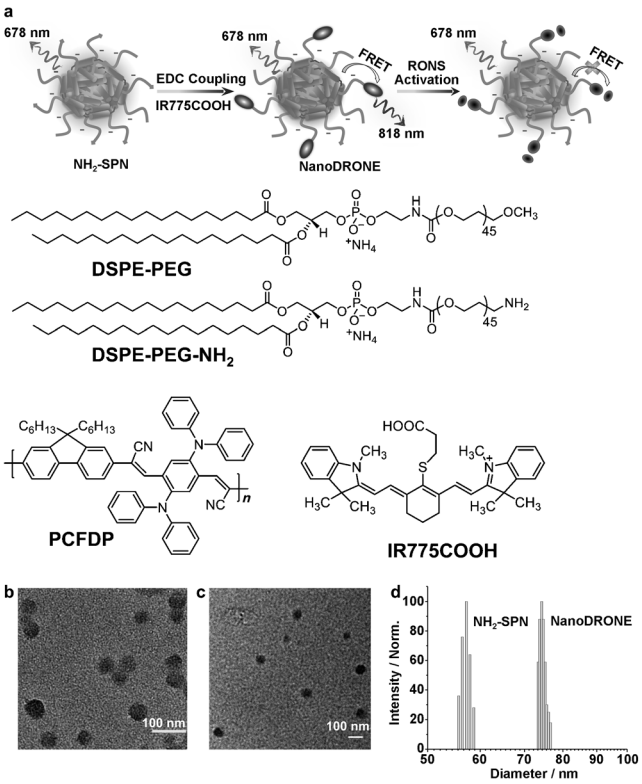

Figure 1. a) Preparation and RONS sensing of NanoDRONE, and the molecular structures of PCFDP, DSPE-PEG, DSPE-PEG-NH_2, and IR775COOH. Representative TEM images of b) NH_2-SPN and c) NanoDRONE. d) Representative DLS profiles of NH_2-SPN and NanoDRONE in 1×PBS (pH 7.4).

[*] Dr. K. Y. Pu,[+] Dr. A. J. Shuhendler,[+] Prof. J. Rao
Molecular Imaging Program at Stanford
Departments of Radiology and Chemistry
Stanford University
1201 Welch Road, Stanford, CA 94305-5484 (USA)
E-mail: jrao@stanford.edu

[+] These authors contributed equally to this work.

[**] This work was supported by the NIH National Cancer Institute (NCI; grant numbers R01CA135294 and R21CA138353A2) and the Stanford University NCI CCNE-T (grant number U54CA119367). We acknowledge the use of the SCi[3] Core Facility at Stanford and the expertise of Pauline Chu in preparing histology samples. A.J.S. also thanks the Susan G. Komen For The Cure for fellowship support.

Supporting information for this article is available on the WWW under http://dx.doi.org/10.1002/anie.201303420.

intensity of SPN and a change in the emission spectrum that provides a RONS-dependent spectral fingerprint. By virtue of poly(ethylene glycol) (PEG) coated nanoarchitecture, NanoDRONE possesses another desirable advantage over small-molecule probes, namely passive targeting in tissues with leaky vasculature through the enhanced permeability and retention (EPR) effect. As leaky vasculature is a hallmark of inflammation,[13] NanoDRONE can effectively accumulate at inflammatory regions, permitting RONS imaging following systemic administration.

The facile synthesis of NanoDRONE proceeds in two steps as illustrated in Figure 1a. We first used a nanoprecipitation method to prepare NH_2-functionalized SPNs (NH_2-SPNs) by choosing a NIR-emissive semiconducting polymer, PCFDP, as the fluorescent polymer and DSPE-PEG and DSPE-PEG-NH_2 as the matrix polymers (PCFDP = [9,9′-dihexyl-2,7-bis(1-cyanovinylene)fluorenylene-*alt*-*co*-2,5-bis(*N*,*N*′-diphenylamino)-1,4-phenylene], DSPE-PEG = 1,2-dimyristoyl-*sn*-glycero-3-phosphoethanolamine-*N*-[methoxy(polyethylene glycol)-2000], and DSPE-PEG-NH_2 = 1,2-distearoyl-*sn*-glycero-3-phosphoethanolamine-*N*-[amino(polyethylene glycol)-2000]). Then, a cyanine dye derivative (IR775COOH), which was recently reported to undergo oxidation-induced degradation in the presence of RONS,[14] was conjugated to the nanoparticle surface through a carbodiimide-activated coupling reaction to afford NanoDRONE. The successful conjugation of IR775COOH was confirmed by agarose gel electrophoresis (see Figure S1 in the Supporting Information). Both NH_2-SPN and NanoDRONE have spherical morphology as shown by TEM (Figure 1b,c). After the conjugation of the positively charged dye to the nanoparticle surface, the average diameter of the nanoparticles increased from 56 nm for NH_2-SPN to 78 nm for NanoDRONE as measured by dynamic light scattering (DLS) (Figure 1d), whereas the zeta potential of NanoDRONE increased from −21 mV for NH_2-SPN to −9 mV. NanoDRONE has high stability in aqueous solution (see Figure S2 in the Supporting Information), attributable to the strong steric repulsion provided by the PEG shell.

NanoDRONE has two absorption peaks at 410 and 788 nm (Figure 2a), corresponding to the SPN core and the fluorophore, respectively. Upon excitation of the SPN core, NanoDRONE exhibits an additional emission peak at 818 nm relative to NH_2-SPN (678 nm; Figure 2b), confirming FRET from the SPN core to the fluorophore on the surface. Moreover, the fluorescence of NanoDRONE at 678 nm was much weaker than that of NH_2-SPN (inset of Figure 2b): the fluorescence quantum yield of NanoDRONE decreased from the original 18% of NH_2-SPN to 3%. However, simple mixing of IR775COOH with NH_2-SPN at the same concentrations did not cause obvious fluorescence change to NH_2-SPN (see Figure S3), which confirms the successful conjugation of the fluorophore to the nanoparticle surface and also highlights its necessity for efficient FRET.

The fluorescence response of NanoDRONE toward RONS is not only determined by the efficacy of the decomposition of the energy acceptor upon reaction with RONS, but also depends on the stability of the energy donor in the presence of RONS. To confirm that SPN is a suitable donor in FRET-based RONS sensing, the fluorescence stability of NH_2-SPN was studied and compared with QD655 and Cy5.5 (Figure 2c). With increasing concentrations of ClO^-, one of the most oxidative RONS, both QD655 and Cy5.5 showed significantly decreased fluorescence, whereas NH_2-SPN was significantly more resistant, showing only slight decreases in its fluorescence. At $[ClO^-] = 14\ \mu M$, the fluorescence of NH_2-SPN only decreases by 9%; in contrast, the fluorescence of Cy5.5 nearly vanished, and QD655 showed a decrease of 86%. In addition to ClO^-, NH_2-SPN was tolerant to other RONS, such as $ONOO^-$, $^{\bullet}OH$, $O_2^{\bullet-}$, $^1O_2$, and H_2O_2 (Figure S4), indicating its superiority over QD655 and Cy5.5 as a reliable and inert energy donor for RONS sensing.

The fluorescence responses of NanoDRONE toward RONS were evaluated in solution under physiological conditions. Figure 3a shows the representative fluorescence spectral changes of NanoDRONE upon addition of RONS such as $ONOO^-$. With increasing concentrations of $ONOO^-$, the emission peak at 678 nm correspondingly increased with the concurrent loss of emission at 818 nm. This is due to the rapid oxidative cleavage of the oligomethine moiety of the FRET acceptor (IR775COOH),[14] which abolishes FRET and recovers the donor fluorescence (SPN) at 678 nm. Thereby, NanoDRONE has a spectral fingerprint that can change from a dual-peak profile (678/818 nm) to a single-peak profile (678 nm) upon RONS activation. Figure 3b summarizes the discriminatory fluorescence responses of NanoDRONE at 678 nm to a number of RONS in N_2-purged phosphate-buffered saline (PBS). The probe emission can be significantly enhanced by $ONOO^-$ (4.0 times), ClO^- (3.6 times), and $^{\bullet}OH$ (2.5 times), and slightly enhanced by $^1O_2$ (1.4 times), $O_2^{\bullet-}$ (1.3 times), and NO (1.2 times), but not by H_2O_2. In PBS without N_2 purging, the intensity incensements are nearly the same for RONS expect for NO (2.9 times), which should be due to the generation of other stronger RONS from the

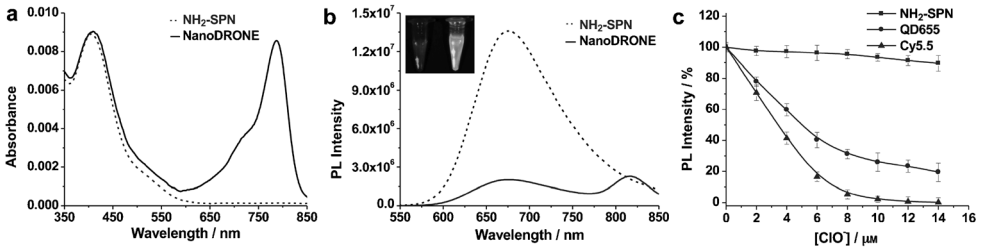

Figure 2. a) UV/Vis absorption and b) fluorescence spectra of NH_2-SPN and NanoDRONE in PBS (30 mM, pH 7.4). c) Fluorescence changes of NH_2-SPN, QD655, and Cy5.5 at 678, 655, and 693 nm, respectively, upon addition of ClO^- in PBS (30 mM, pH 7.4). $[NH_2\text{-SPN}] = [Cy5.5] = 1.0\ \mu g$; $[QD655] = 20$ nM. Excitation wavelengths for NH_2-SPN, QD655, and Cy5.5 are 405, 500, and 630 nm, respectively. Error bars represent the standard deviation from three measurements.

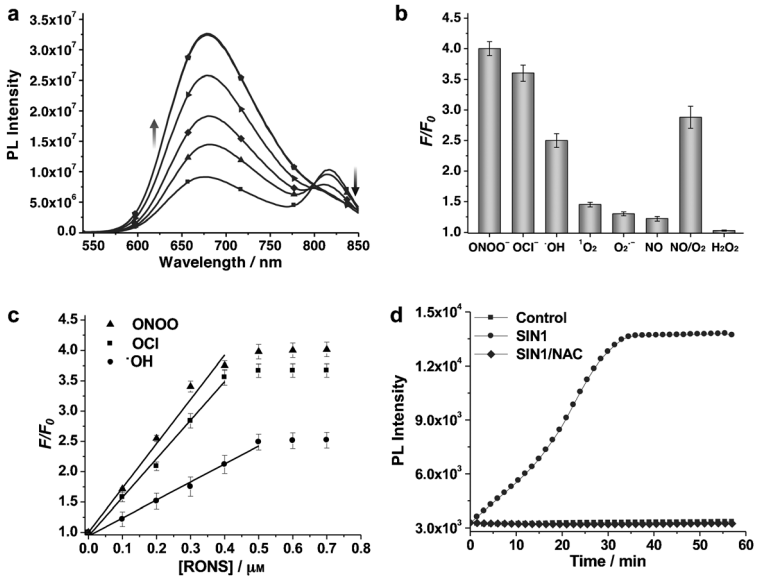

Figure 3. a) Fluorescence spectra of NanoDRONE in PBS (30 mM, pH 7.4) in the absence or presence of $ONOO^-$ at concentrations of 0.1, 0.2, 0.3, 0.4, or 0.5 μM. b) Fluorescence responses of NanoDRONE (0.1 μg mL^{-1}) toward RONS in nitrogen-purged PBS (pH 7.4). F and F_0 stand for the fluorescence intensities at λ_{em} = 678 nm in the presence and absence of RONS (1 μM), respectively. Excitation at 405 nm. c) F/F_0 as a function of the RONS concentration. d) Time course of the fluorescence of NanoDRONE at 678 nm in the absence or presence of SIN1 or SIN1/NAC in PBS (30 mM, pH 7.4). [NanoDRONE] = 0.1 μg mL^{-1}; [SIN1] = 5 μM; [NAC] = 50 μM. Error bars represent the standard deviation from three measurements.

autooxidation between NO and O_2. In addition, the fluorescence enhancement of NanoDRONE shows an excellent linear correlation with the concentration of the RONS such as $ONOO^-$, ClO^- and ·OH ($R^2 > 0.99$; Figure 3c). The limit of detection for those RONS is determined to be about 10 nM in solution, which is comparable to or even lower than previously reported probes.[2–7] The combination of the RONS sensitivity of NanoDRONE with its nearly unchanged fluorescence after RONS activation under physiological conditions (Figure S6) makes it feasible for in vivo RONS imaging.

The ability of NanoDRONE to detect RONS was further examined in solution under bioinspired conditions of RONS generation. 3-Morpholinosydnonimine (SIN1), which spontaneously releases NO and $O_2^{\bullet-}$ to form $ONOO^-$ in aqueous solution, was used to mimic the generation of $ONOO^-$ by macrophages. With increasing incubation time with SIN1, the fluorescence of NanoDRONE at 678 nm gradually increased to a maximum (4 times) at 35 minutes (Figure 3d). This is consistent with the fluorescence enhancement observed by the direct addition of $ONOO^-$ into the probe solution. This activation of NanoDRONE was prevented in the presence of *N*-acetylcysteine (NAC), a general antioxidant.[15] The fluorescence of the nanoprobe remained unchanged after incubation with either SIN1 (Figure 3d) or ClO^- (Figure S7), revealing the successful scavenging of both $ONOO^-$ and ClO^-, respectively, by NAC.

NanoDRONE was then applied to detect endogenously generated RONS in cultured cell types relevant to inflammation. RAW264.7, a murine macrophage cell line, showed very weak fluorescence after incubation with NanoDRONE in its resting state (Figure 4a). To mimic the inflammatory condition that activates resting tissue macrophages, RAW264.7 cells were successively pre-treated with bacterial cell wall lipopolysaccharide (LPS) and phorbol 12-myristate 13-acetate (PMA) to elicit the elevated production of RONS such as $ONOO^-$ and ClO^-.[16] With LPS/PMA stimulation, strong fluorescence was observed from the cells (Figure 4b), indicating the activation of the nanoprobe by RONS under conditions relevant to inflammation. When NAC, a free-radical scavenger with high membrane permeability, was used to treat the cells along with LPS/PMA stimulation, no obvious fluorescence was observed after incubation with NanoDRONE (Figure 4c). This indicates that NAC scavenges endogenously generated RONS from macrophage cells and effectively inhibits the activation of NanoDRONE, similarly to that observed in solution. Additionally, NanoDRONE was found to be nontoxic to three tested cell lines including RAW264.7, RWPE-1, and HeLa cells (Figure S8). These in vitro data clearly demonstrate that NanoDRONE can efficiently detect RONS produced in stressed cells.

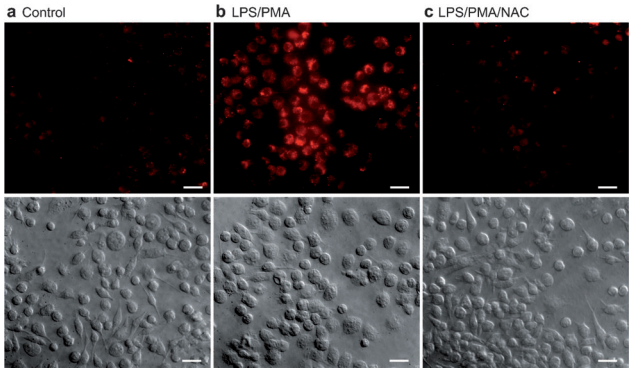

Figure 4. Fluorescence and differential interference contrast (DIC) images of live murine macrophages (RAW 264.7) incubated with NanoDRONE (1.5 μg mL^{-1}, 3 h) before imaging: a) nontreated cells, b) cells successively treated with LPS (2 h) and PMA (0.5 h), and c) cells pretreated with NAC 2 h before treated with LPS (2 h) and PMA (0.5 h), followed with NAC for 1 h. [LPS] = 1 μg mL^{-1}; [PMA] = 5 μg mL^{-1}; [NAC] = 1 mM. Scale bars: 20 μm.

NanoDRONE was applied to the imaging of RONS in living mice in an animal model of peritonitis induced by intraperitoneal (i.p.) injection of LPS. NanoDRONE was administered by i.p. injection 4 h after the injection of saline or LPS (Figure 5a), and fluorescence images were acquired 30 minutes after particle administration. The fluorescence intensities of the LPS-treated mice were 2.7 times higher than those of the saline-treated mice (Figure 5b). In addition, exposure of the peritoneal cavity during necropsy confirmed

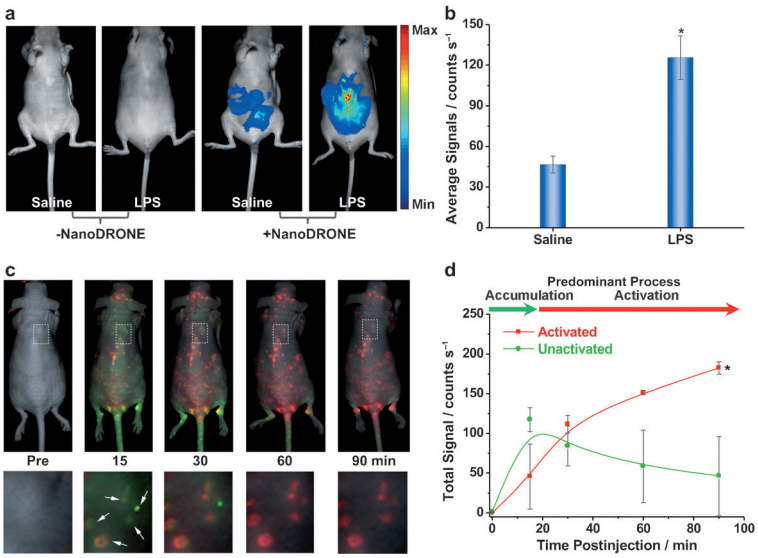

Figure 5. a) In vivo imaging of RONS with NanoDRONE in a LPS-induced acute peritonitis mouse model. Saline ($n=4$) and LPS ($n=4$) were administered i.p., followed 4 h later by i.p. administration of NanoDRONE. Images were acquired before and 30 minutes after particle administration. b) The quantified average fluorescence intensities of the peritoneal cavity for each treatment group. *indicates statistically significant increase of fluorescence intensity relative to the control groups ($p<0.05$). c) Imaging RONS with NanoDRONE in mice with spontaneous systemic *C. bovis* bacterial infection. Overlaid images of activated (red) and unactivated (green) NanoDRONE following i.v. administration to mice with spontaneous infections ($n=4$). Enlargements of the regions indicated by dashed white boxes are given below each corresponding image. White arrows indicate localized regions of bacterial infection. d) Quantification of activated (red) and nonactivated (green) NanoDRONE fluorescence over time. *Significantly different change in fluorescence between unactivated and activated nanoprobe ($p<0.05$).

the isolation of the observed fluorescence to the peritoneum and not the overlying skin (Figure S9).

The in vivo application of existing RONS probes in living mouse models are mainly limited to local administration by i.p. injection, possibly owing to unfavorable pharmacokinetics and biodistribution associated with these probes.[2–7] Thus, NanoDRONE was injected intravenously (i.v.) to test its suitability for systemic administration. We found that NanoDRONE had a relatively long circulation time (about 6 h) and thus a favorable biodistribution (Figure S10), which resulted in dynamic accumulation in the liver, kidney, gastrointestinal tract, skin, heart, and brain, all of which decreased with time (Figure S10a). Notably, organs of the reticuloendothelial system (RES) such as the liver and spleen did not display higher nanoparticle uptake than non-reticuloendothelial tissues, suggesting the ability of NanoDRONE to evade RES uptake. The relatively long circulation time and favorable biodistribution of NanoDRONE, in conjunction with the lack of any overt systemic toxicity of the particle ingredients revealing its amenability to i.v. administration for in vivo imaging of RONS in whole animals.

Since inflammation can be induced by pathogen-associated molecular patterns (PAMPs) following bacterial infection, NanoDRONE was evaluated for the systemic imaging of the RONS pool following i.v. administration in mouse models of spontaneous *Corynebacterium bovis* (*C. bovis*) bacterial infection. Nude mice are susceptible to skin infection by *C. bovis*,[17] which results in inflammation localized to regions of infection. As NanoDRONE has a spectral fingerprint dependent on their state of activation (Figure 2a), hyperspectral in vivo fluorescence imaging can be employed to deconvolve unactivated from activated probe states in live animals (SI, Figure S11). Following the intravenous injection of NanoDRONE to mice spontaneously infected by *C. bovis*, fluorescence images were taken, and signals from unactivated (illustrated in pseudo-green color) and activated (illustrated in pseudo-red color) probes were deconvolved (Figure S12a), overlaid (Figure 5c), and quantified (Figure 5d). NanoDRONE was found to first specifically accumulate in the infected foci within 15 minutes through the EPR effect, and then progressively be induced to change from unactivated (green) to activated (red) states by microenvironmental RONS in the bacterial infection regions, with complete probe activation by 60 minutes. A histological analysis also showed specific accumulation of NanoDRONE to infected regions (Figure S12b in SI), which further proves its propensity for passive targeting to inflammatory microenvironments via the EPR effect following systemic administration.

In summary, we have developed a SPN-based NIR nanoprobe by taking advantage of the RONS-inert property of SPN in conjunction with a RONS-sensitive cyanine derivative for imaging of RONS. With high physiological stability, good biodistribution and long circulation half-life, and passive targeting to inflammatory regions, this nanoprobe allows for detection of RONS in the microenvironment of inflammation using systemic administration. Additionally, its RONS-dependent fluorescence spectral fingerprint in the NIR region permits real-time probe tracking and differentiation of probe activation from accumulation in living mice. Our probe design thus potentially provides more advantages for in vivo RONS imaging as compared with "off-on" imaging probes that can only be seen once activated. The current probe does not show specificity over $ONOO^-$, ClO^-, and $^{\cdot}OH$, and is more suitable for detection of the RONS pool at inflammation sites in living animals. However, the modular core–shell probe design allows the use of other RONS-selective NIR fluorophores as the energy acceptor to generate nanoprobes with specificity for individual RONS.[18] Thus, this SPN nanoplatform has the potential to provide real-time, in situ information regarding the RONS status of diseases.

Received: April 23, 2013
Revised: July 14, 2013
Published online: August 13, 2013

Keywords: biosensors · imaging agents · nanoparticles · polymers · reactive oxygen and nitrogen species

[1] a) D. L. Carden, D. N. Granger, *J. Pathol.* **2000**, *190*, 255; b) R. Medzhitov, *Nature* **2008**, *454*, 428; c) H. W. Querfurth, F. M. LaFerla, *N. Engl. J. Med.* **2010**, *362*, 329.

[2] J. Chan, S. C. Dodani, C. J. Chang, *Nat. Chem.* **2012**, *4*, 973.

[3] a) M. H. Lim, D. Xu, S. J. Lippard, *Nat. Chem. Biol.* **2006**, *2*, 375; b) Y. Koide, Y. Urano, S. Kenmoku, H. Kojima, T. Nagano, *J. Am. Chem. Soc.* **2007**, *129*, 10324; c) K. Kundu, S. F. Knight, N. Willett, S. Lee, W. R. Taylor, N. Murthy, *Angew. Chem.* **2009**, *121*, 305; *Angew. Chem. Int. Ed.* **2009**, *48*, 299.

[4] V. V. Belousov, A. F. Fradkov, K. A. Lukyanov, D. B. Staroverov, K. S. Shakhbazov, A. V. Terskikh, S. Lukyanov, *Nat. Methods* **2006**, *3*, 281.

[5] H. Jin, D. A. Heller, M. Kalbacova, J. H. Kim, J. Zhang, A. A. Boghossian, N. Maheshri, M. S. Strano, *Nat. Nanotechnol.* **2010**, *5*, 302.

[6] M. C. Mancini, B. A. Kairdolf, A. M. Smith, S. Nie, *J. Am. Chem. Soc.* **2008**, *130*, 10836.

[7] P. Panizzi, M. Nahrendorf, M. Wildgruber, P. Waterman, J.-L. Figueiredo, E. Aikawa, J. McCarthy, R. Weissleder, S. A. Hilderbrand, *J. Am. Chem. Soc.* **2009**, *131*, 15739.

[8] a) J. Oakes, P. Gratton, *J. Chem. Soc. Perkin Trans. 1* **1998**, *2*, 2201; b) A. P. F. M. de Urzedo, C. C. Nascentes, M. E. R. Diniz, R. R. Catharino, M. N. Eberlin, R. Augusti, *Rapid Commun. Mass Spectrom.* **2007**, *21*, 1893; c) A. Toutchkine, D. V. Nguyen, K. M. Hahn, *Org. Lett.* **2007**, *9*, 2775; d) Y. Yan, S. Wang, Z. Liu, H. Wang, D. Huang, *Anal. Chem.* **2010**, *82*, 9775.

[9] a) C. Wu, C. Szymanski, Z. Cain, J. McNeill, *J. Am. Chem. Soc.* **2007**, *129*, 12904; b) J. H. Moon, W. McDaniel, P. MacLean, L. E. Hancock, *Angew. Chem.* **2007**, *119*, 8371; *Angew. Chem. Int. Ed.* **2007**, *46*, 8223; c) J. Pecher, S. Mecking, *Chem. Rev.* **2010**, *110*, 6260; d) K. Y. Pu, K. Li, B. Liu, *Chem. Mater.* **2012**, *24*, 6736; e) C. Zhu, L. Liu, Q. Yang, F. Lv, S. Wang, *Chem. Rev.* **2012**, *112*, 4687; f) K. Y. Pu, B. Liu, *Adv. Funct. Mater.* **2011**, *21*, 3408; g) C. Wu, D. T. Chiu, *Angew. Chem.* **2013**, *125*, 3164; *Angew. Chem. Int. Ed.* **2013**, *52*, 3086.

[10] L. P. Fernando, P. K. Kandel, J. B. Yu, J. McNeill, P. C. Ackroyd, K. A. Christensen, *Biomacromolecules* **2010**, *11*, 2675.

[11] a) S. Kim, C. K. Lim, J. Na, Y. D. Lee, K. Kim, K. Choi, J. F. Leary, I. C. Kwon, *Chem. Commun.* **2010**, *46*, 1617; b) C. Wu, S. Hansen, Q. Hou, J. Yu, M. Zeigler, Y. Jin, D. Burnham, J. McNeill, J. Olson, D. T. Chiu, *Angew. Chem.* **2011**, *123*, 3492; *Angew. Chem. Int. Ed.* **2011**, *50*, 3430; c) K. Li, D. Ding, D. Huo, K. Y. Pu, N. N. P. Thao, Y. Hu, Z. Li, B. Liu, *Adv. Funct. Mater.* **2012**, *22*, 3107.

[12] L. Xiong, A. J. Shuhendler, J. Rao, *Nat. Commun.* **2012**, *3*, 1193.

[13] N. M. Goldenberg, B. E. Steinberg, A. S. Slutsky, W. L. Lee, *Sci. Transl. Med.* **2011**, *3*, 88ps25.

[14] D. Oushiki, H. Kojima, T. Terai, M. Arita, K. Hanaoka, Y. Urano, T. Nagano, *J. Am. Chem. Soc.* **2010**, *132*, 2795.

[15] a) M. Zafarullah, W. Q. Li, J. Sylvester, M. Ahmad, *Cell. Mol. Life Sci.* **2003**, *60*, 6; b) K.-C. Sheng, G. A. Pietersz, C. K. Tang, P. A. Ramsland, V. Apostolopoulos, *J. Immunol.* **2010**, *184*, 2863; c) V. M. Victor, M. Rocha, M. De La Fuente, *Free Radical Res.* **2003**, *37*, 919.

[16] a) S. Hashioka, Y. H. Han, S. Fujii, T. Kato, A. Monji, H. Utsumi, M. Sawada, H. Nakanishi, S. Kanba, *Neurochem. Int.* **2007**, *50*, 499; b) C. Bergt, G. Marsche, U. Panzenboeck, J. W. Heinecke, E. Malle, W. Sattler, *Eur. J. Biochem.* **2001**, *268*, 3523.

[17] H. N. Burr, N. S. Lipman, J. R. White, J. Zheng, F. R. Wolf, *J. Am. Assoc. Lab. Anim. Sci.* **2011**, *50*, 378.

[18] a) J. Tian, H. Chen, L. Zhuo, Y. Xie, N. Li, B. Tang, *Chem. Eur. J.* **2011**, *17*, 6626; b) L. Yuan, W. Lin, Y. Yang, H. Chen, *J. Am. Chem. Soc.* **2012**, *134*, 1200.